A Reconstruction Approach to Scatterometer Wind Vector Field Retrieval

Brent A. Williams, *Member, IEEE*, and David G. Long, *Fellow, IEEE*

***Abstract*—This paper approaches wind field estimation from scatterometer measurements as the inversion of a noisy nonlinear sampling operation. The forward sampling model is presented and made discrete for practical purposes. Generally, the wind estimation problem is ill-posed at high resolution, which means that there are more parameters to estimate than measurements. A Bayesian approach based on maximum *a posteriori* (MAP) estimation is proposed to regularize the problem. This allows the simultaneous estimation of the regular samples of the high-resolution wind vector field directly from the noisy aperture-filtered backscatter σ^0 measurements. The MAP reconstruction approach is applied to the SeaWinds scatterometer, the examples are presented, and the results are compared to standard products. The MAP reconstruction method produces results that are consistent with standard products while preserving the higher spatial resolution information. The MAP estimates result in a similar resolution to the standard ultrahigh-resolution processing method but with a lower bias and a lower variability in the estimates.**

***Index Terms*—Irregular sampling, maximum *a posteriori* (MAP) estimation, reconstruction, scatterometry, wind estimation.**

I. Introduction

A SCATTEROMETER is a radar that measures the normalized radar cross section (σ^0) of the Earth's surface. Over the ocean, the backscattered signal is related to the wind through a geophysical model function (GMF). Each σ^0 measurement contains information about the wind, averaged over an area. Scatterometers make several measurements over the same spatial region with different geometries, polarizations, and, possibly, frequencies. These different "flavors" of measurements can be combined to estimate the wind vector field over the ocean. Several methods of estimating the wind field from the σ^0 measurements have been proposed, each having their limitations and imposing different assumptions.

Conventionally, the wind field is estimated on a pointwise or wind vector cell (WVC) basis [1]–[4], i.e., the scatterometer swath is partitioned into discrete wind WVCs, and a single wind vector (or a set of ambiguous wind vectors) is separately estimated for each WVC. A separate ambiguity removal step is then applied to the entire swath to resolve a unique wind field [5], [6]. The scatterometer data may be assimilated directly into the numerical weather predictions using a variational analysis approach [7]–[12]. The standard scatterometer processing employs a drop-in-the-bucket gridding technique using only the measurements whose centers fall into a particular WVC to estimate the wind for that WVC. This approach essentially assumes a uniform wind vector field over the WVC, although more sophisticated wind estimation methods exist, which can account for subcell variability [13]. Ultrahigh-resolution (UHR) products have been obtained by reconstructing the σ^0 fields of each flavor separately and then performing pointwise wind retrieval on a high-resolution grid [14], [15]. Both the standard and UHR pointwise methods impose implicit assumptions and neglect the spatial correlation between WVCs in the wind retrieval step. Although the ambiguity selection methods can impose a fieldwise structure and can account for some signal correlation after wind retrieval, the noise correlation between WVCs (or covariance) is often neglected in the implicit assumptions of both wind retrieval and ambiguity selection. Since the spatial response functions of the scatterometer measurements generally extend into multiple WVCs, the covariance of the estimates may not be diagonal across the WVCs with a more general inversion procedure. An alternative approach which relies neither on binning nor on σ^0 reconstruction and which incorporates the spatial relationship between the measurements (both the signal correlation and noise covariance) is to reconstruct the entire wind field directly from the σ^0 measurements, i.e., fieldwise wind estimation.

Fieldwise wind estimation has been explored in the past with model-based methods [8], [16]–[18]. In this approach, the wind field model parameters are estimated from the σ^0 measurements, and the wind field estimate is then computed from the model parameter estimates. Fieldwise approaches also result in ambiguous wind field estimates that require ambiguity removal. Note that, if the wind field is not in the span of the model, the estimated wind may not be the closest wind field in the space to the true wind field. Furthermore, model-based methods impose structure (i.e., the model) on the wind fields, which often results in smoothed wind estimates and which may be inappropriate for a particular application.

Another fieldwise approach that does not impose a restrictive fieldwise model is based on the inversion of the sampling operation. This is the basis of several σ^0 image reconstruction methods [19], [20]. The conventional scatterometer image reconstruction approaches are designed to produce high-resolution σ^0 images. However, they can be adapted for the wind field reconstruction problem to deal appropriately with the scatterometer noise and the nonlinear relationship between the wind and σ^0. For example, [21] and [22] developed an approach to simultaneously estimate the regularly spaced samples of the σ^0 field from the scatterometer measurements,

Manuscript received February 25, 2010; revised October 19, 2010; accepted November 16, 2010. Date of publication January 27, 2011; date of current version May 20, 2011.

B. A. Williams is with the Jet Propulsion Laboratory, Pasadena, CA 91109 USA (e-mail: williams@mers.byu.edu; Brent.A.Williams@jpl.nasa.gov).

D. G. Long is with the Brigham Young University, Provo, UT 84602 USA (e-mail: long@ee.byu.edu).

Digital Object Identifier 10.1109/TGRS.2010.2100402

which deals directly with the scatterometer noise model, and this approach can be extended to deal with the nonlinear GMF.

This paper considers the alternate fieldwise approach to reconstruct the wind vector field directly from the σ^0 measurements. This paper approaches the scatterometer wind estimation problem as the inversion of a noisy nonlinear sampling operation, i.e., as a noisy inverse problem. A more general scatterometer sampling model is presented. A Bayesian maximum *a posteriori* (MAP) estimation method is proposed to reconstruct the wind vector field at a high resolution directly from the noisy σ^0 measurements. The focus of this paper is on developing the theory and a practical implementation for the wind inversion step, leaving the issues of ambiguity removal and noise versus resolution tradeoffs within the new theoretical framework for future investigation. The new approach generalizes and unifies the other wind estimation approaches. The conventional drop-in-the-bucket, UHR, and model-based approaches can be expressed as simplified special cases of the new method. The reconstruction approach is applied to retrieve the high-resolution wind fields from the SeaWinds scatterometer. The new results are compared to the conventional products.

This paper is organized as follows. Section II presents the forward scatterometer sampling operation and shows that it can be made discrete under reasonable assumptions. Section III presents a method for wind field estimation from noisy scatterometer measurements. Section IV considers the relationship between conventional approaches and the new method. Section V applies the new approach to the SeaWinds scatterometer. Finally, Section VI summarizes the results and concludes this paper.

II. Forward Model

The forward model or sampling operation describes the relationship between the wind field and the scatterometer measurements. This relationship is required in estimating the wind field from the scatterometer measurements. This section presents the scatterometer sampling model. The background on sampling and aperture-filtered sampling is presented, the scatterometer sampling operation is stated, the forward operator is made discrete, and the sample spacing or pixel resolution is considered.

A. Sampling

Sampling is the process of converting a continuous signal into a sequence. Sampling in a Hilbert space can be represented as a sequence of inner products of a signal with sampling functions (i.e., aperture functions). Conventional sampling can be represented as a vector of inner products with Dirac delta functions. In a bandlimited space, this is equivalent to sampling with sinc function apertures [23]. More generally, sampling can be done with irregularly spaced aperture functions with different shapes. Such samples are called aperture-filtered samples [22], [24]. In scatterometry, the aperture function is the measurement spatial response function due to the antenna pattern and processing, and sampling is the process of making σ^0 measurements.

Wind scatterometry is an application of aperture-filtered sampling in the sense that each σ^0 measurement represents an aperture-filtered sample of a continuous σ^0 field. However, each measurement samples a different σ^0 field (i.e., measurements are made with different geometries). Over the ocean, the σ^0 fields sampled by a scatterometer are related nonlinearly to the underlying wind field through the GMF, which also depends on incidence angle, azimuth angle, polarization, and frequency.

B. Scatterometer Sampling Model

Scatterometers measure the backscattered power from the Earth's surface, averaged over the antenna gain pattern. This power measurement is scaled to produce the normalized radar cross section [25]. The measurement of a given scatterometer pulse is partitioned into several "slice" measurements using range/Doppler processing or pulse compression [1], [2], [26]. The spatial response functions (i.e., aperture functions) of the slice measurements vary in shape and location. Neglecting noise, the power in the return echo for a particular slice measurement $P_{r,i}$ can be represented by the area-extensive form of the radar equation [27]

$$P_{r,i} = \frac{\lambda^2}{(4\pi)^3} \int \frac{P_{t,i}(x) G_i^2(x) \sigma_{t,i}^0(x)}{\mathcal{R}_i^4(x)} dx$$

where λ is the wavelength, x is a 2-D spatial variable, $\sigma_{t,i}^0(x)$ is the "true" or noise-free spatially distributed σ^0 field associated with the ith measurement, $P_{t,i}(x)$ is the transmitted power, $G_i(x)$ is the gain pattern of the slice point target response function, and $\mathcal{R}_i(x)$ is the slant range to the scattering surface. The σ^0 measurement for a particular slice i is obtained by normalizing the measurement of P_r by the so called X factor

$$X_i = \frac{\lambda^2}{(4\pi)^3} \int \frac{P_{t,i}(x) G_i^2(x)}{\mathcal{R}_i^4(x)} dx$$

which allows the ith noise-free σ^0 measurement $\sigma_{t,i}^0$ to be expressed as

$$\sigma_{t,i}^0 = \frac{P_{r,i}}{X_i} = \int \frac{P_{t,i}(x) G_i^2(x) \sigma_{t,i}^0(x)}{\mathcal{R}_i^4(x) \int \frac{P_{t,i}(y) G_i^2(y)}{\mathcal{R}_i^4(y)} dy} dx$$

$$= \int A_i(x) \sigma_{t,i}^0(x) dx$$

where $A_i(x)$ represents the slice spatial response function (i.e., aperture function) for slice measurement i. Note that we use the notation $\sigma_{t,i}^0$ to represent a scalar measurement and append (x) to denote a continuous field associated with the measurement (e.g., $\sigma_{t,i}^0(x)$).

Over the ocean, the $\sigma_{t,i}^0(x)$ fields are related to the wind vector field $\vec{U}(x)$ through the GMF

$$\sigma_{t,i}^0(x) = \text{gmf}\left(\vec{U}(x), \theta_i(x), \psi_i(x), pol_i, f_i\right) = \text{gmf}_i\left(\vec{U}(x)\right)$$

where $\theta_i(x)$, $\psi_i(x)$, pol_i, and f_i are the incidence angle field, azimuth angle field, polarization, and frequency corresponding to the ith slice measurement, respectively. For convenience,

these arguments of the GMF are dropped in the rest of this paper, resulting in the more compact notation $\text{gmf}_i(\vec{U}(x))$. Scatterometers make several measurements with different look geometries over the same spatial region. Stacking the multiple measurements into a vector, the scatterometer sampling model is expressed as

$$\vec{\sigma}_t^0 = \begin{bmatrix} \sigma_{t,1}^0 \\ \vdots \\ \sigma_{t,N}^0 \end{bmatrix} = \begin{bmatrix} \int A_1(x)\text{gmf}_1\left(\vec{U}(x)\right)dx \\ \vdots \\ \int A_N(x)\text{gmf}_N\left(\vec{U}(x)\right)dx \end{bmatrix} = \mathcal{T}\left(\vec{U}(x)\right) \quad (1)$$

where $\mathcal{T}$ is a nonlinear sampling operator that maps the wind field to the noise-free slice measurements.

Equation (1) states the forward model (i.e., projecting the wind to the σ^0 measurements). Wind field reconstruction involves solving the inverse problem (i.e., estimating the wind from the σ^0 measurements). In theory, the sampling operation can be inverted using constrained optimization (see Appendix A). However, in order to simplify the problem and to deal with noise appropriately, the problem is discretely solved.

C. Discrete Model

Here, the sampling operation is transformed into a discrete operation on conventional samples of the wind field (i.e., the forward operation is made discrete). The wind field can be made discrete by assuming that it is bandlimited. However, in order to make the sampling operation discrete, the integrals in (1) must be expressible as summations. Furthermore, not only the wind field but also the σ^0 fields $\sigma_{t,i}^0(x)$ corresponding to each measurement i must be bandlimited.

For a general nonlinear function, assuming that the wind field is bandlimited does not necessarily force the corresponding σ^0 fields to be bandlimited. Nevertheless, the GMF can be expressed in such a way that the σ^0 fields are guaranteed to be bandlimited but with a potentially different bandlimit than the wind.

The GMF is an empirical function that can be approximated by a finite power series. In Appendix B, it is shown that, if the wind field has bandlimited components and the nonlinear GMF can be represented by a finite power series, then the relationship between the bandlimit of the σ^0 fields ω_σ and the bandlimit of the wind field components ω_{U_1} and ω_{U_2} is (see Appendix B)

$$\omega_\sigma \leq N_1\omega_{U_1} + N_2\omega_{U_2} + \omega_a \quad (2)$$

where N_1 and N_2 correspond to the order of the power series for the wind vector components and ω_a is the bandlimit of the power series coefficients.

The inequality in (2) states that the σ^0 fields are bounded above by a weighted sum of the wind field component bandlimits, which also implies that the σ^0 fields may have higher frequency content than either of the individual wind field components. For example, if $N_1 = N_2 = 2$, $\omega_a = 0$, and $\omega_{U_1} = \omega_{U_2} \equiv \omega_U$, then $\omega_\sigma \leq 4\omega_U$, and the bandlimit of the σ^0 field may be up to four times the bandlimit of the individual wind field components. This relationship suggests that the regular sample spacing required to represent the σ^0 fields may be finer than the regular sample spacing required to represent the wind field components. Thus, an oversampled version of the wind field with the assumed bandlimit should be projected through the discrete version of $\mathcal{T}$ when numerically calculating the forward projection. However, relatively small errors may result from expressing the σ^0 fields on the same wind field grid (see Appendix B).

Thus, if the wind field components are bandlimited, the σ^0 fields are also bandlimited, and the sampling operator can be made discrete. The discrete sampling operation can be expressed as

$$\vec{\sigma}_t^0 = \begin{bmatrix} \sum_x A_1[x]\text{gmf}_1\left(\vec{U}[x]\right) \\ \vdots \\ \sum_x A_N[x]\text{gmf}_N\left(\vec{U}[x]\right) \end{bmatrix} = \mathbf{T}\left(\vec{U}[x]\right) \quad (3)$$

where the square brackets $[x]$ represent the regularly spaced samples on an up-sampled version of the wind field grid (since the σ^0 bandlimit is higher than the wind field bandlimit) and $\mathbf{T}$ is the discrete version of the nonlinear sampling operator $\mathcal{T}$. The Nyquist samples of the wind field, denoted as $\vec{U}[x']$, are related to the samples on the higher resolution grid by $\vec{U}[x] = \mathbf{H}\vec{U}[x']$, where $\mathbf{H}$ is the up-sampling operator.

D. Wind Field Bandlimit and Sample Spacing

As noted, the sampling operator can be made discrete by assuming a bandlimited wind field. However, the bandlimit to assume must be considered. The assumed bandlimit determines the regular sample spacing required to represent the wind field with that bandlimit. This sample spacing provides the pixel resolution on which to reconstruct the wind fields.

Determining the wind bandlimit and the regular sample spacing is much more complicated than the case of linear aperture-filtered sampling with bandlimited aperture functions. In the linear case, the sample spacing is determined directly from the highest bandlimit of the aperture functions [22]. With the pointwise nonlinear constraint introduced by the GMF, it may be possible to recover a higher frequency content than the bandlimit of the aperture functions (see Appendix A). Therefore, the bandlimit or signal structure imposed is based on the knowledge of the wind spectrum.

Fortunately, wind generally has a red spectrum that falls off approximately as one over the wavenumber squared [28]. This allows for the imposition of a relatively low bandlimit, without introducing significant aliasing on average. Nevertheless, for particular wind features, such as storms or fronts, the wavenumber spectrum may have a significant high-frequency energy. In general, a better result may be obtained by assuming a high bandlimit rather than potentially introducing aliasing by assuming a bandlimit that is too low. This suggests that reconstruction must be done on the highest resolution grid that is practical and that lower resolution estimates must be obtained by low-pass filtering the estimated wind. However,

when considering noise and the biased estimators, it may be beneficial to retrieve at a lower resolution (at least where the winds are smooth) in order to reduce the systematic errors that may not average out by low-pass filtering the noisier high-resolution estimates. Nevertheless, for this paper, a high-resolution gridding is employed, deferring the noise and bias versus resolution tradeoff for a future paper.

III. Wind Field Reconstruction From Noisy σ^0 Measurements

Wind retrieval from scatterometer measurements is a noisy inverse problem that can be solved using an estimation theory approach. Here, wind field reconstruction from noisy σ^0 measurements over the ocean is considered. A scatterometer noise model is reviewed. A MAP reconstruction estimator is proposed for wind field reconstruction. An appropriate prior that is used to regularize the problem is presented. An approach for practical implementation is also described.

A. Noise Distribution

The noise distribution for a scatterometer measurement is modeled as a Gaussian random variable with a mean that is the true or noise-free value and with a variance that is a quadratic function of the mean [29], [30]. This variance formulation incorporates fading and receiver noise. With this noise model, the vector of the noisy σ^0 measurements $\vec{\sigma}^0_m$ can be expressed as

$$\vec{\sigma}^0_m = \vec{\sigma}^0_t + \vec{\nu}$$

where $\vec{\sigma}^0_t = \mathbf{T}(\mathbf{H}\vec{U}[x'])$ and $\vec{\nu}$ is a zero-mean Gaussian random vector with a diagonal covariance $\mathbf{R}$. The diagonal terms of the covariance $R_{i,i}$ can be written as

$$R_{i,i} = \alpha_i \left(\sigma^0_{t,i}\right)^2 + \beta_i \sigma^0_{t,i} + \gamma_i$$

where $\sigma^0_{t,i}$ is the ith component of $\vec{\sigma}^0_t$ and α_i, β_i, and γ_i are the functions of the scatterometer design and the measured noise power. Note that the aforementioned expression assumes that the GMF is a deterministic mapping. The uncertainty in the GMF (or geophysical noise [31]) may be included by modifying the random vector $\vec{\nu}$.

For this paper, we assume that the geophysical noise is negligible, and we use the Gaussian noise model described earlier. This results in the likelihood function

$$f\left(\vec{\sigma}^0_m|\vec{\sigma}^0_t\right) = \frac{\exp\left\{\left(\vec{\sigma}^0_m - \vec{\sigma}^0_t\right)^T \mathbf{R}^{-1}\left(\vec{\sigma}^0_m - \vec{\sigma}^0_t\right)\right\}}{(2\pi)^{N/2}|\mathbf{R}|^{1/2}}. \quad (4)$$

Note that $f(\vec{\sigma}^0_m|\vec{\sigma}^0_t)$ may also be expressed as $f(\vec{\sigma}^0_m|\vec{U}[x'])$ since $\vec{\sigma}^0_t = \mathbf{T}(\mathbf{H}\vec{U}[x'])$.

A common approach in estimating the parameters of a distribution is maximum-likelihood (ML) estimation. However, at UHR, the scatterometer wind field estimation problem is generally ill-posed (i.e., there are more parameters to estimate than measurements). To regularize the problem, we propose a Bayesian approach which employs a prior distribution.

B. MAP Reconstruction Estimator

Because of the nonlinearity of the GMF, the shape of the noise distribution with respect to the wind is generally multimodal [31]. A MAP estimator can deal with the potential ambiguity caused by this. MAP estimation is Bayesian estimation with a uniform loss function [32] and is similar to ML estimation, but it also incorporates the prior distribution. The MAP estimator can be expressed as

$$\hat{\vec{U}}_{MAP}[x'] = \arg\max_{\vec{U}[x']} f\left(\vec{\sigma}^0_m|\vec{\sigma}^0_t\right) f\left(\vec{U}[x']\right)$$

where $\vec{\sigma}^0_m$ is the noisy measurement vector, $f(\vec{\sigma}^0_m|\vec{\sigma}^0_t)$ is the likelihood function defined in (4), and $f(\vec{U}[x'])$ is a prior distribution. Note that $f(\vec{U}[x'])$ need not be a direct prior of the wind vector field. For example, the prior can be a distribution of some function of the wind field. In practice, the MAP log-likelihood function

$$\log f\left(\vec{\sigma}^0_m|\vec{\sigma}^0_t\right) + \log f\left(\vec{U}[x']\right)$$

is used as the MAP objective function.

C. Prior Distributions

Prior distributions can be empirically derived from the data or can be chosen to apply additional constraints. For wind scatterometry, prior distributions can both regularize the inverse problem and aid in ambiguity selection [33], [34]. Prior distributions can also be employed to force the wind estimates to be consistent with other wind field estimates with potentially different resolutions.

For the purpose of this paper, we desire to impose a prior that regularizes the problem, without imposing much structure on the wind fields and without relying too heavily on the external data. In order to regularize the problem, we apply a prior that is independent from pixel to pixel. Although a wind field prior may be used, we apply the prior in the σ^0 field domain since it is difficult to obtain a useful direction prior without an external data source. Imposing a prior on the σ^0 fields in this manner can be viewed as estimating the σ^0 fields via the wind, i.e., we reconstruct the σ^0 fields that are consistent with an underlying wind field and simultaneously produce a wind field estimate.

We assume that each pixel of each σ^0 field has the mean of the obtained scatterometer measurement and a finite variance. The Gaussian distribution is the maximum entropy distribution for a given mean and variance, i.e., it imposes the least amount of structure of all distributions with a given mean and variance [35]. Therefore, each pixel of each σ^0 field is assumed to be an independent Gaussian random variable with a mean corresponding to the aperture-filtered σ^0 measurement and a given variance. More precisely, the prior can be expressed as

$$f\left(\vec{U}[x']\right) = \prod_{i,x'} f\left(\sigma^0_{t,i}[x']\right) = \prod_{i,x'} f\left(\mathrm{gmf}_i\left(\vec{U}[x']\right)\right) \quad (5)$$

where each $f(\mathrm{gmf}_i(\vec{U}[x']))$ is

$$f\left(\mathrm{gmf}_i\left(\vec{U}[x']\right)\right) = \frac{1}{\sqrt{2\pi}p}\exp\left\{\frac{\left(\sigma^0_{m,i} - \mathrm{gmf}_i\left(\vec{U}[x']\right)\right)^2}{-2p^2}\right\} \tag{6}$$

where p^2 is the variance. Note that, for all of the pixels of the σ^0 field for a given measurement i, the mean $\sigma^0_{m,i}$ of this prior is constant. Thus, this prior also acts as a smoothing filter on the σ^0 fields and on the wind estimates. The variance p^2 is left as a tuning parameter to trade off the spatial resolution for a reduced variability of the estimates. For this paper, we set p to 10^{-7} based on the preliminary empirical observations, leaving a more detailed noise versus resolution tradeoff analysis for future investigation.

Note that the form of $f(\vec{U}[x'])$ in (5) and (6) is similar in form to the measurement noise distribution $f(\vec{\sigma}^0_m|\vec{\sigma}^0_t)$ in (4), assuming a white process across the WVCs as well as across the different measurements i. Thus, this prior regularizes the ill-posed problem by adding a diagonal to the Fisher information matrix of the fieldwise ML estimation problem [36]. This property justifies the use of this prior as a regularization term without requiring knowledge of the actual distribution of the wind fields or their corresponding σ^0 fields. This approach allows the estimation of the fine-scale features (such as storms and fronts) that are relatively rare and isolated compared to larger scale structures. Nevertheless, applying a prior corresponding to the actual distribution of the wind fields may be more appropriate for certain applications.

D. Implementation

Because of the nonlinearity of the GMF and the structure of the noise, the MAP objective function is multimodal. The local maxima represent the fieldwise ambiguous winds. Although it is theoretically possible to find every local maxima and to report them as wind field ambiguities, this is difficult because of the high number of parameters in the wind field reconstruction problem.

For convenience, we employ a gradient search method initializing with an up-sampled result of the standard resolution product. This results in a single wind field estimate. The initialization field effectively acts as an ambiguity selection step since the new method generally converges to a wind field ambiguity close to the initialization field. This implementation can be viewed as a resolution enhancement procedure on the standard resolution product. Alternative initialization fields may be obtained from UHR processing, model-based wind field estimation from the σ^0 data, or data from external sources. Note that the wind field may be estimated in the meridional and zonal components or in the speed and direction components. We search along the gradient with respect to the wind speed and direction components since it is simpler to search numerically due to the structure of the objective function. The gradient of the MAP objective function is provided in Appendix C.

IV. Connections Between Approaches

The new approach solves the general inverse problem by regularizing via a prior. The conventional approaches, which apply assumptions and approximations to solve the problem, can be expressed as simplified special cases of the new method. The implicit assumptions made by the drop-in-the-bucket and UHR methods have the effect of regularizing the wind inversion problem by enabling pointwise wind field estimation. This section explores the relationship between the new approach and the standard drop-in-the-bucket, UHR, and model-based approaches.

A. Drop-in-the-Bucket Approach

First, consider the drop-in-the-bucket approach. This approach uses multiple measurements whose aperture function centers fall into a WVC to independently estimate a wind vector for that cell [37]. In relation to the sampling model in (1), this can be viewed as assuming that the wind field is piecewise constant over the WVCs and that the aperture functions are delta functions, i.e., under the implicit assumptions, each row of the sampling model can be expressed as

$$\sigma^0_{d,i} = \int \delta(x - x_i)\mathrm{gmf}_i\left(\vec{U}(x)\right)dx = \mathrm{gmf}_i\left(\vec{U}(x_i)\right) \tag{7}$$

where x_i is the center of the aperture function for measurement i and $\vec{U}(x_i) = \vec{U}(x_j)$ for all x_i, x_j in the same WVC. We use the notation $\sigma^0_{d,i}$ to represent the ith σ^0 measurement for the drop-in-the-bucket method. The vector of the σ^0 measurements for the drop-in-the-bucket method is expressed as $\vec{\sigma}^0_d$. Note that, since the true wind field is not piecewise constant and the aperture functions are not delta functions, the drop-in-the-bucket technique, in effect, solves a different problem than the original. The errors introduced by the implicit assumptions made using the drop-in-the-bucket methods can be evaluated by

$$\begin{aligned}
&\left\|\vec{\sigma}^0_t - \vec{\sigma}^0_d\right\|_{L_1} \\
&\quad = \sum_i \left|\sigma^0_{t,i} - \vec{\sigma}^0_{d,i}\right| \\
&\quad = \sum_i \left|\int A_i(x)\mathrm{gmf}_i\left(\vec{U}(x)\right)dx - \mathrm{gmf}_i\left(\vec{U}(x_i)\right)\right| \\
&\quad = \sum_i \left|\int A_i(x)\left[\mathrm{gmf}_i\left(\vec{U}(x)\right) - \mathrm{gmf}_i\left(\vec{U}(x_i)\right)\right]dx\right| \\
&\quad \le \sum_i \int A_i(x)\left|\mathrm{gmf}_i\left(\vec{U}(x)\right) - \mathrm{gmf}_i\left(\vec{U}(x_i)\right)\right|dx.
\end{aligned}$$

If the wind field is relatively smooth, $|\mathrm{gmf}_i(\vec{U}(x)) - \mathrm{gmf}_i(\vec{U}(x_i))|$ is generally small for each i, and the L_1 normed difference between the forward projections is small. However, for wind fields with a significant small-scale structure, the normed difference may be large, resulting in biases in the wind estimates.

While the drop-in-the-bucket sampling operation differs from the new method, the noise model is the same, i.e., the same fundamental measurements are used to estimate the wind field for both cases, but the manner in which the measurements are combined in wind retrieval differs due to the assumptions imposed about the wind field itself. The drop-in-the-bucket method has a similar expression for the likelihood function $f(\vec{\sigma}_m^0|\vec{\sigma}_d^0)$, as expressed in (4), but with $\vec{\sigma}_t^0$ replaced by $\vec{\sigma}_d^0$. Note that the GMF is empirically derived from the data obtained from winds with all scales (i.e., including winds with finer scale structures than either the WVC size or the width of the slice response functions). This suggests that there may be a difference between the GMF that is inside the integral and outside the integral in (7), which implies that a high-resolution GMF may be more appropriate for the new approach.

Now, it is shown that the MAP reconstruction method for estimating the wind reduces to the conventional method, assuming the drop-in-the-bucket forward model and a particular prior. First, suppose that we apply the new fieldwise approach to estimate the wind from the σ^0 measurements, assuming the drop-in-the-bucket forward operation. The assumption that the wind field is piecewise constant makes the problem discrete, albeit in a different way than assuming that the wind fields are bandlimited. To solve this discrete problem using the MAP reconstruction approach, a gradient search is used. With the drop-in-the-bucket forward model, the gradient of the likelihood function defined in Appendix C (11) reduces to

$$\frac{\partial \log f\left(\vec{\sigma}_m^0|\vec{U}[x']\right)}{\partial U_j[x]} = \begin{cases} \sum_i K_i \frac{\partial \text{gmf}_i(\vec{U}[x])}{\partial U_j[x]}, & \text{if } x' = x \\ 0, & \text{otherwise} \end{cases}$$

where the square brackets $[x]$ represent the regular sampling of the piecewise constant wind field (i.e., one sample per WVC). Note that the partial derivative of the likelihood function with respect to the wind at a particular WVC is not a function of the wind in other WVCs. This implies that the wind vector at each WVC can be independently estimated (i.e., pointwise).

Note that the aforementioned expression is the gradient of the likelihood function without the prior. As long as some measurements fall into every WVC, the wind can be estimated pointwise for each WVC without a prior (i.e., the Fisher information matrix is diagonal and not singular). Thus, the implicit assumptions in the modified forward model effectively regularize the problem. If no prior is imposed (or, equivalently, if a noninformative prior is used), the MAP reconstruction approach reduces to conventional processing when assuming the drop-in-the-bucket forward model. We note, however, that the new approach provides more control of how the problem is regularized and allows for higher resolution wind estimates than what is possible with the conventional drop-in-the-bucket methods.

B. UHR Approach

The UHR approach assumes a similar forward model as in (1) but modifies it slightly by making an important assumption. UHR processing assumes that the measurements of a similar geometry (and same polarization and frequency) sample the same wind-dependent σ^0 field.

More precisely, each row of the UHR sampling operation is expressed as

$$\sigma_{UHR,i}^0 = \int A_i(x) \text{gmf}_f\left(\vec{U}(x)\right) dx$$

where $\text{gmf}_f(\vec{U}(x))$ represents the σ^0 field of a given flavor (e.g., consecutive measurements from the same beam). Under the UHR assumption, each $\sigma_{UHR,i}^0$ of a particular flavor samples the same $\text{gmf}_f(\vec{U}(x))$. The multiple measurements of a given flavor are combined to reconstruct the σ^0 field of a given flavor, and this is done for each different flavor. The wind is then estimated pointwise from the reconstructed σ^0 fields [14].

Although the assumption is that multiple measurements sample the same σ^0 field, each measurement actually samples a slightly different σ^0 field because each measurement views the surface with a slightly different geometry. The error introduced by this assumption can be evaluated as

$$\begin{aligned} &\left\|\vec{\sigma}_t^0 - \vec{\sigma}_{UHR}^0\right\|_{L_1} \\ &\quad = \sum_i \left|\sigma_{t,i}^0 - \vec{\sigma}_{UHR,i}^0\right| \\ &\quad = \sum_i \left| \int A_i(x) \text{gmf}_i\left(\vec{U}(x)\right) dx \right. \\ &\qquad\qquad \left. - \int A_i(x) \text{gmf}_f\left(\vec{U}(x)\right) dx \right| \\ &\quad = \sum_i \left| \int A_i(x) \left[\text{gmf}_i\left(\vec{U}(x)\right) - \text{gmf}_f\left(\vec{U}(x)\right)\right] dx \right| \\ &\quad \le \sum_i \int A_i(x) \left|\text{gmf}_i\left(\vec{U}(x)\right) - \text{gmf}_f\left(\vec{U}(x)\right)\right| dx \end{aligned}$$

where $\vec{\sigma}_{UHR}^0$ is the vector of measurements assuming the UHR forward model and $\text{gmf}_f(\vec{U}(x))$ is the σ^0 field assuming the geometry of flavor f. The normed difference between the forward projections is relatively small if the change in the GMF with respect to the differences in the geometry between the actual measurements i and the assumed look geometry is small over the main lobe of $A_i(x)$. For scatterometer designs with narrow measurement spatial response functions, this assumption is appropriate, but for scatterometer systems with broad measurement response functions, this assumption may result in significant bias errors.

The noise model assumed for UHR processing differs from the standard noise model. Although the UHR noise model is derived from the standard noise model, the UHR model assumes that each pixel is statistically independent, resulting in a diagonal covariance matrix. Also, the mean of the distributions for each pixel is assumed to be the true σ^0 value at the given pixel (i.e., $\sigma_{t,i}^0[x] = \text{gmf}_i(\vec{U}[x])$ for pixel x).

Note that, if the covariance is assumed to be diagonal, it is generally nonsingular (except possibly if there are WVCs that happen to be in a null of every aperture function). This implicit assumption regularizes the problem, making pointwise

estimation possible without imposing a prior. If no prior is imposed (or, equivalently, if a noninformative prior is used), MAP reconstruction reduces to pointwise UHR estimation when assuming the UHR forward operation and noise model.

The actual noise distribution of the reconstructed σ^0 fields has a correlation among adjacent WVCs due to the measurement overlap, resulting in a nondiagonal covariance matrix. Although the UHR assumptions simplify the problem and result in useful estimates, assuming that the covariance is diagonal may result in artifacts when the actual correlation is significant.

The modifications to the noise model used in UHR processing regularize the problem and make pointwise retrieval possible, but they are somewhat ad hoc. An alternate method may be to regularize the problem by adding a diagonal to the singular covariance matrix. In fact, this is equivalent to applying an independent Gaussian prior to each pixel of the reconstructed σ^0 fields and performing MAP estimation on a fieldwise basis, which is similar to what is proposed earlier. This suggests that, for systems where measurements of a similar flavor can be combined, the prior in (6) may be modified by replacing the mean $\sigma^0_{m,i}$ with the reconstructed σ^0 value for a given pixel.

C. Model-Based Approach

Model-based estimation assumes that the true wind field is contained in the span of the wind field model. The model parameters are estimated from the measurements, and then, a wind field estimate is computed from the model parameter estimates. Generally, a model is chosen so that there are fewer parameters to estimate than measurements, thus regularizing the problem. The parameters are conventionally estimated using ML estimation [16]–[18]. Note that assuming that the wind field is in the span of a wind field model is equivalent to imposing a uniform prior over the range space of the wind field model. Thus, the model-based methods can also be expressed as a special case of the MAP reconstruction approach.

V. Application to SeaWinds

This section considers the application of the MAP wind reconstruction method to the SeaWinds scatterometer. Here, the background on the sensor is provided, the examples are presented, and the MAP reconstruction estimates are compared to conventional products. Simulation is employed to analyze the quality of the estimates.

A. SeaWinds Background

SeaWinds is a Ku-band scanning pencil-beam scatterometer. Two beams (v-pol and h-pol) at two different nominal incidence angles are employed to produce a wide swath with a sufficient azimuth diversity to infer wind direction. Range/Doppler filtering is employed to obtain several σ^0 measurements ("slices") for each radar pulse [1]. The aperture function of each slice σ^0 measurement is a function of the antenna pattern and the range/Doppler processing. In practice, each aperture function is often approximated by a binary mask (i.e., a mask with ones within the 6-dB main lobe and zeros outside) [38].

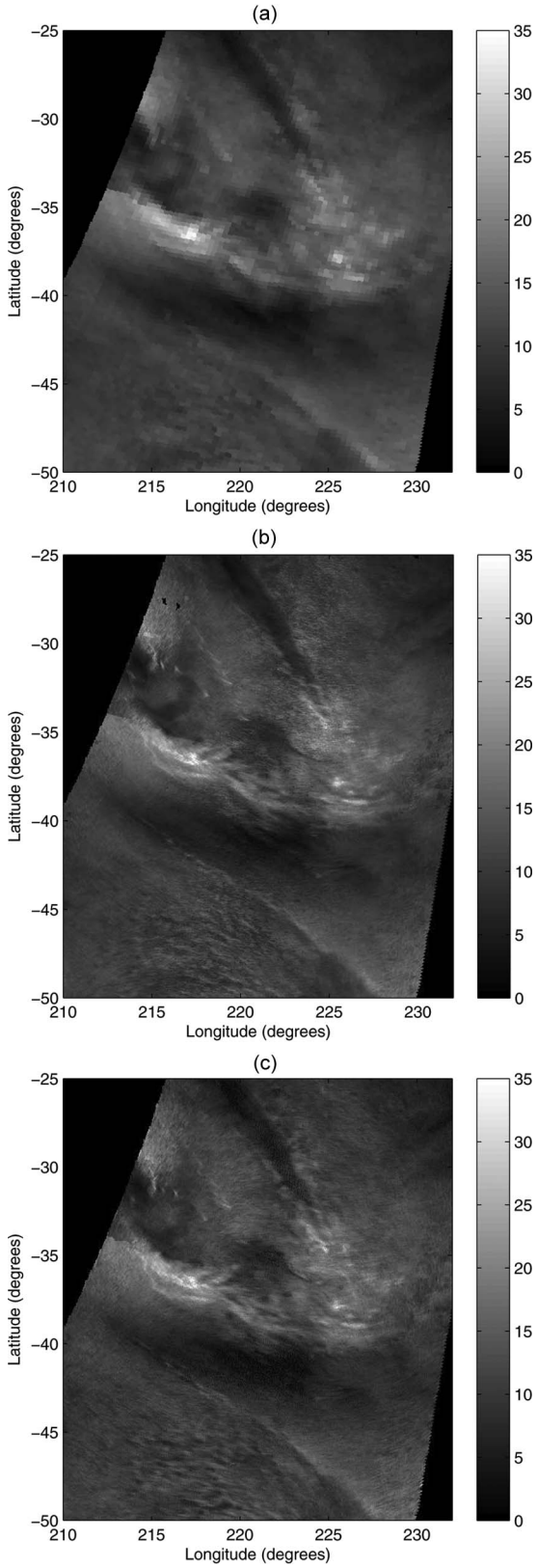

Fig. 1. Wind speed fields (in meters per second) from (a) L2B, (b) UHR, and (c) MAP reconstruction.

For SeaWinds, the wind is conventionally estimated on 25- (L2B), 12.5- (L2BH), and 2.5-km grids (UHR). For the L2B product, the slices of a given pulse are first averaged together into egg measurements, and the eggs whose centers fall into a

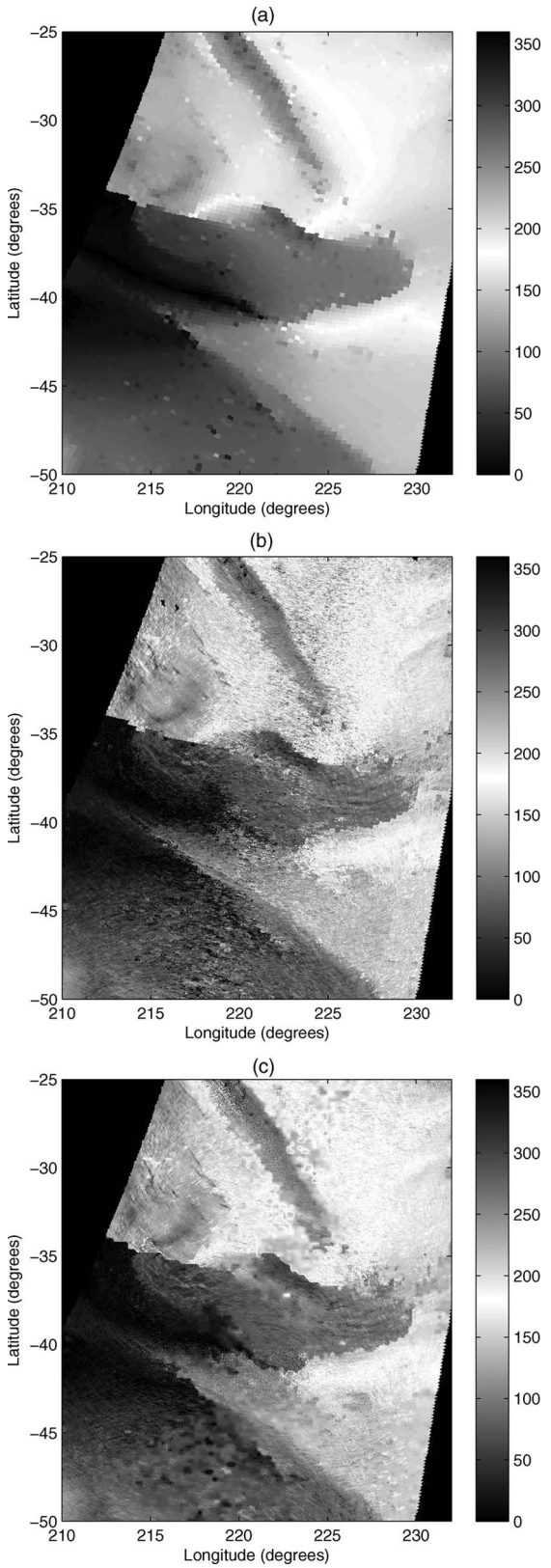

Fig. 2. Wind direction fields (in degrees) relative to north from (a) L2B, (b) UHR, and (c) MAP reconstruction.

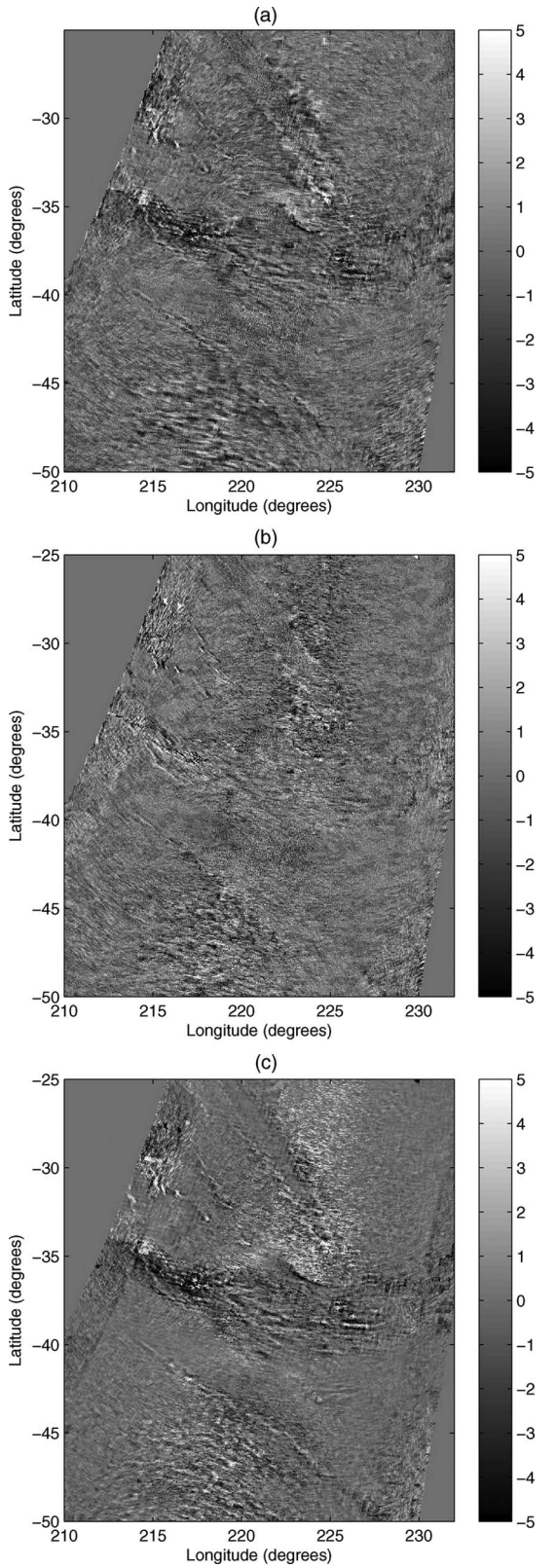

Fig. 3. Wind speed difference fields (in meters per second) from the (a) difference between MAP and L2B, (b) difference between MAP and UHR, and (c) difference between UHR and L2B.

25-km WVC are used to estimate the wind vector for that WVC [1]. A similar procedure is done for the L2BH product, and only the measurements are binned on a 12.5-km grid [1]. UHR processing first reconstructs four σ^0 fields [one for each flavor (v-pol, h-pol, and fore- and aft- looking)] onto a 2.5-km grid using a weighted average of all of the slice σ^0 values weighted by the respective aperture functions [19], [20]. The wind is then

estimated pointwise from the reconstructed σ^0 fields [14]. We compare the results of these different methods with the new MAP reconstruction method.

B. Example

Figs. 1 and 2 show an example of wind field reconstruction from the SeaWinds scatterometer for a wind field with relatively small scale features. The L2B, UHR, and MAP estimated wind speed fields are shown in Fig. 1, while the direction fields are shown in Fig. 2. The new method improves the resolution over the L2B product, producing a wind field that is similar to the UHR field but with less noise.

Figs. 3 and 4 show the speed difference fields and direction difference fields between the various methods, respectively. The differences between the MAP and L2B fields, the MAP and UHR fields, and the UHR and L2B fields are all shown. These images suggest that the MAP estimates are consistent with the L2B and UHR estimates throughout the swath. The UHR speed and direction estimates are noisy in the nadir region, while the MAP direction estimates appear less noisy. Note that the differences between the UHR and L2B, and the MAP and L2B wind estimates are also due, in part, to the differing resolutions of the products.

C. Validation

It is difficult to evaluate the quality of the wind estimates without an independent set of collocated data of a similar resolution. Lacking such data, we compare the MAP reconstruction results to the conventional low resolution results and to the UHR product for 20 SeaWinds passes in the south Atlantic (i.e., a $6 \times 6^\circ$ window around latitude -30 and longitude -130). The south Atlantic is chosen for convenience to avoid the tropics where rain contamination is significant. Tables I and II show the speed and direction mean difference, the standard deviation (STD) of the difference, and the root-mean-squared (rms) difference between the MAP reconstructed and L2B winds, between the UHR and L2B winds, and between the MAP reconstructed and UHR winds. For Table I, the L2B winds are up-sampled (using nearest neighbor interpolation) to the high-resolution grid, while for Table II, the MAP and UHR winds are averaged down (using a vector average) to the L2B resolution. The results suggest that the MAP reconstruction method is consistent with the standard SeaWinds product and with the UHR product. Note that both ML and MAP estimation may result in biased estimates of the wind, which may be different for the different retrieval methods. Thus, systematic biases may occur. Even so, the mean difference (or bias) with respect to the L2B is low for both UHR and MAP wind estimation. The STD and rms differences suggest that the MAP estimates are generally less noisy than the UHR products.

D. Simulation

To further investigate the performance of the new method, we employ the Monte Carlo simulation. The estimates of the bias and variance of the estimates of the L2B, UHR, and MAP reconstruction wind retrieval methods are also obtained using the simulation.

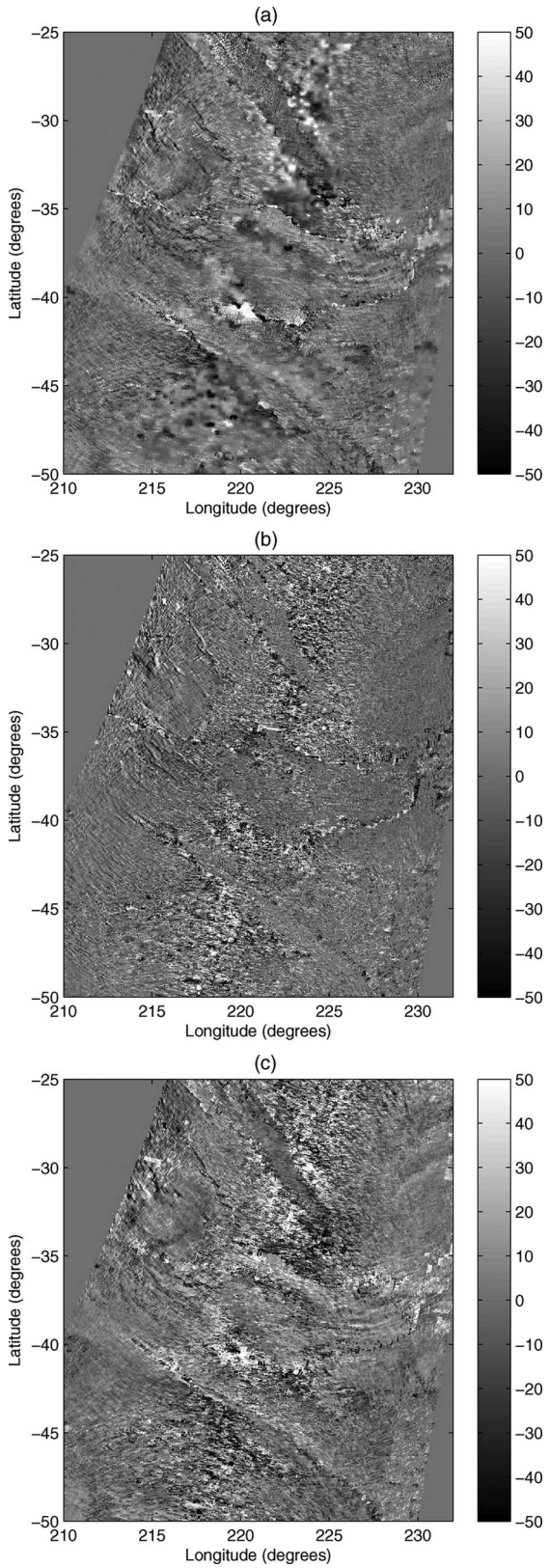

Fig. 4. Wind direction difference fields (in degrees) (a) between MAP and L2B, (b) between MAP and UHR, and (c) between UHR and L2B.

Comprehensive simulation and analysis are beyond the scope of this paper. Here, we analyze the results from a particular

TABLE I
MEAN DIFFERENCE, STD OF THE DIFFERENCE, AND RMS DIFFERENCE BETWEEN THE MAP AND L2B AND BETWEEN THE MAP AND UHR ESTIMATED WIND SPEEDS AND DIRECTIONS AT UHR RESOLUTION (AVERAGED OVER 20 PASSES IN THE SOUTH ATLANTIC)

	Mean	STD	RMS
MAP and L2B speed	-0.46	1.32	1.40
UHR and L2B speed	-0.23	1.53	1.55
MAP and UHR speed	-0.24	1.40	1.42
MAP and L2B dir	-1.78	17.03	17.13
UHR and L2B dir	0.22	26.08	26.08
MAP and UHR dir	-2.01	27.09	27.16

TABLE II
MEAN DIFFERENCE, STD OF THE DIFFERENCE, AND RMS DIFFERENCE BETWEEN THE MAP AND L2B AND BETWEEN THE MAP AND UHR ESTIMATED WIND SPEEDS AND DIRECTIONS AT L2B RESOLUTION (AVERAGED OVER 20 PASSES IN THE SOUTH ATLANTIC)

	Mean	STD	RMS
MAP and L2B speed	-0.98	1.14	1.50
UHR and L2B speed	-1.26	1.22	1.76
MAP and UHR speed	0.28	0.63	0.69
MAP and L2B dir	-1.98	8.38	8.60
UHR and L2B dir	-1.40	9.26	9.37
MAP and UHR dir	-0.58	5.93	5.96

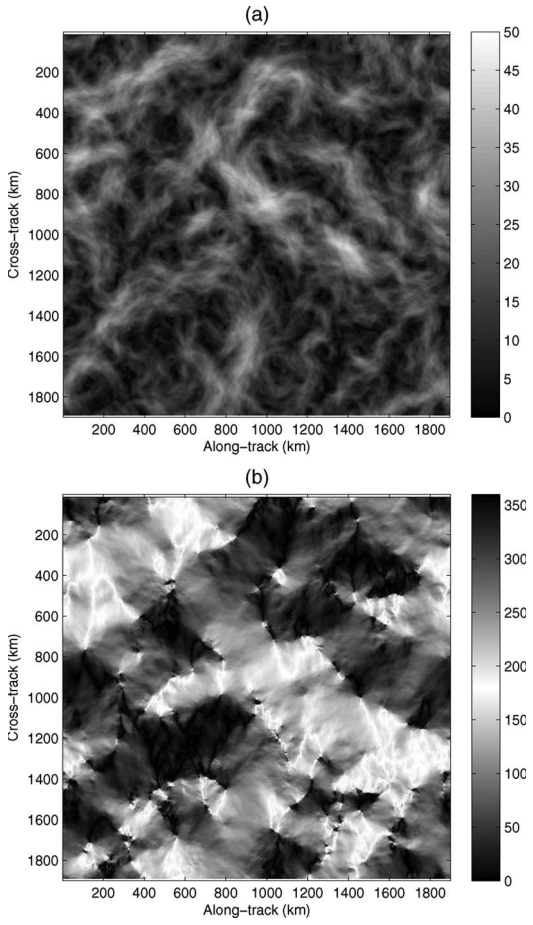

Fig. 5. Simulated (a) wind speed field (in meters per second) and (b) wind direction field (in degrees).

wind field with 100 independent noise realizations. We generate a simulated wind field that has a wavenumber spectrum that falls off as one over the wavenumber squared. Fig. 5 shows the wind speed and direction field used in the simulation. Although this wind field may not be realistic, it exhibits the small-scale structure that is necessary to test the resolution of the estimates.

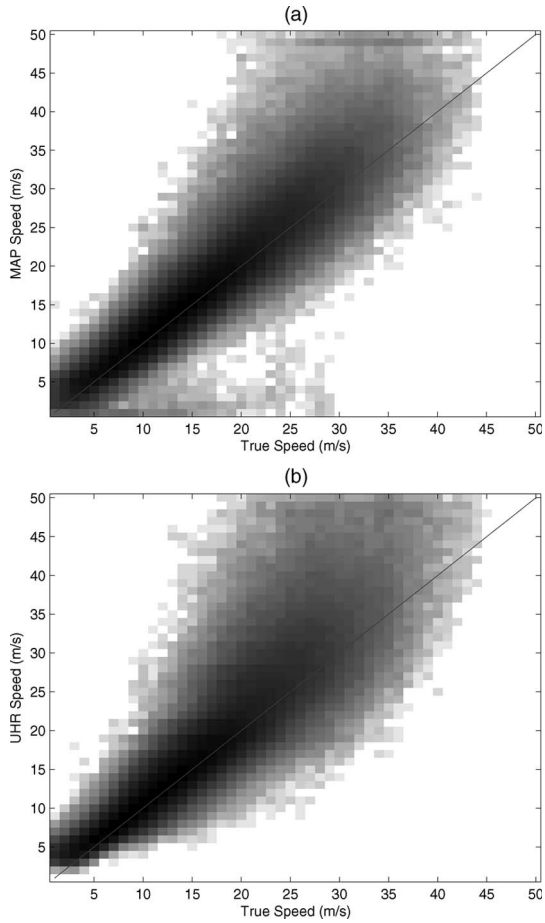

Fig. 6. Scatter density plots of the wind speed obtained in the simulation for (a) MAP and (b) UHR.

Figs. 6 and 7 show the scatter density plots of the MAP and UHR estimates compared to the true wind for the wind speed and direction, respectively, for a particular noise realization. The plots suggest that the MAP direction estimates are less noisy than the UHR estimates. The MAP speed estimates of the high wind speeds have a slightly lower variability than the UHR estimates, while the variability at low wind speeds is higher.

Figs. 8 and 9 show the bias of the wind speed and direction estimates, respectively, for the MAP and UHR methods. For both methods, higher wind speeds tend to produce a larger bias, although the bias of the MAP reconstruction estimates is less severe than the UHR estimates. In the swath edges, the structure of the bias seems to be different from the inner swath. The direction estimates are relatively unbiased, except in the frontal features.

Figs. 10 and 11 show the STD of the wind speed and direction estimates, respectively, for the MAP and UHR methods. As expected, the MAP estimates of the high wind speeds have a lower STD than the UHR estimates. The STD of the direction fields is much different for the UHR and MAP estimates. In the nadir region, the UHR direction estimates have a large STD, whereas the MAP estimates have a relatively low STD all throughout the swath.

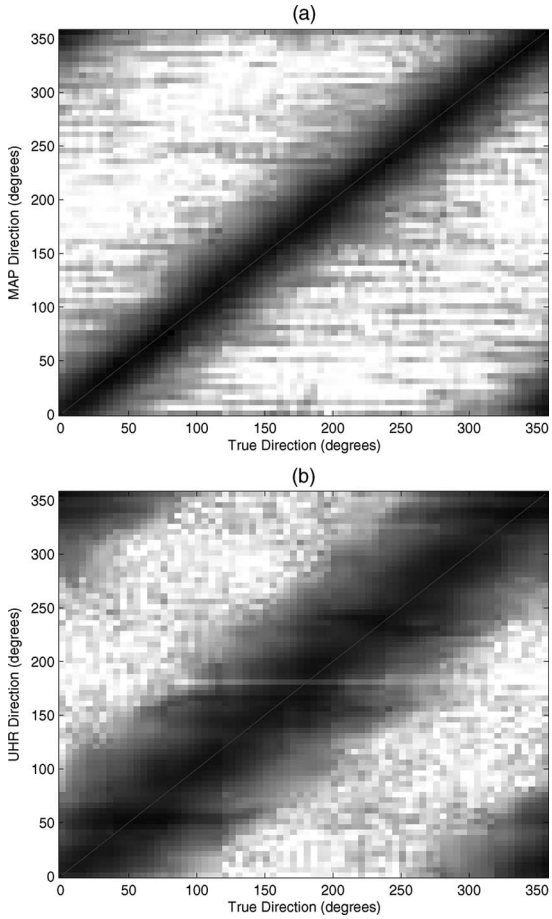

Fig. 7. Scatter density plots of the wind direction obtained in the simulation for (a) MAP and (b) UHR.

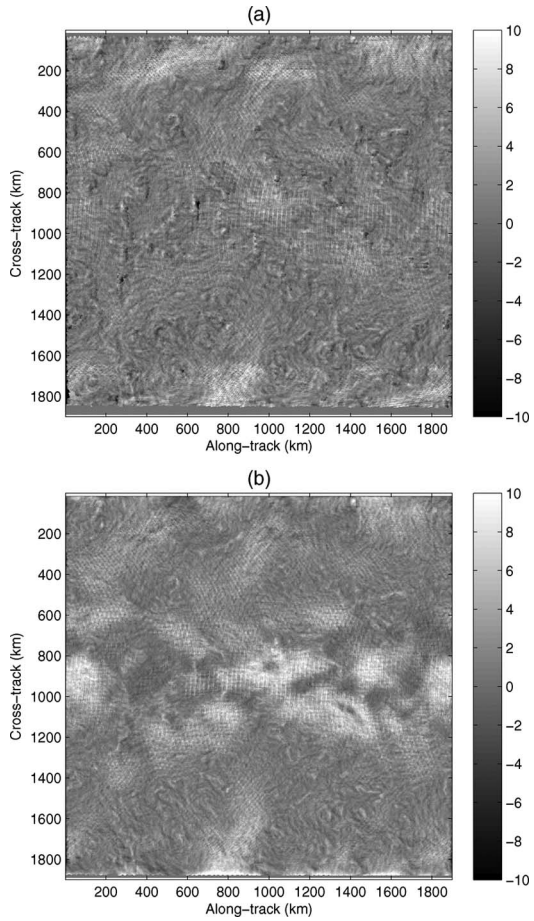

Fig. 8. Bias of the wind speed estimates (in meters per second) for (a) MAP and (b) UHR.

VI. Conclusion

This paper has approached the scatterometer wind field estimation problem in a novel way. Wind field estimation is performed on a fieldwise basis without imposing a low-order model. MAP estimation is employed to estimate the regularly-spaced samples of the wind field at UHR. The method is applied to the SeaWinds scatterometer, and the results are compared to standard products. The MAP reconstruction method is consistent with low-resolution standard products, but it provides higher resolution information. For SeaWinds, the MAP reconstruction estimates are consistent with the UHR estimates, but they have less noise.

Future research will include a more rigorous validation of the MAP reconstruction product for the SeaWinds scatterometer. Also, the approach will be applied to the operational scatterometer data, such as the advanced scatterometer, and will be adapted for a near real-time UHR product. The MAP reconstruction approach will also be extended to simultaneously reconstruct the wind and rain vector fields from the scatterometer measurements. Near the coastal regions, the MAP wind reconstruction approach will be combined with the σ^0 image reconstruction approach developed in [22] to simultaneously reconstruct the wind field over the ocean and the σ^0 image over the land in order to develop an improved coastal product.

Appendix A
Inversion of the Continuous Noise-Free Forward Operator

In theory, the continuous sampling operation can be inverted using constrained optimization. To do this, we define a metric $d(\vec{U}(x), \vec{z}(x))$ over the wind field domain to optimize, subject to a consistent forward sampling operation $\vec{\sigma}_t^0 = \mathcal{T}(\vec{U}(x))$. The metric $d(\vec{U}(x), \vec{z}(x))$ is a measure of the distance between the wind field and some vector field $\vec{z}(x)$. For example, the metric may be a normed error such as the L_2-norm, and $\vec{z}(x)$ may be some expected wind field such as a numerical weather predicted wind field or the zero vector field (e.g., $d(\vec{U}(x), \vec{z}(x)) = \|\vec{U}(x) - \vec{z}(x)\|^2 = \sum_k \int |U_k(x) - z_k(x)|^2 dx$).

To find the optima, the Lagrangian

$$L = d\left(\vec{U}(x), \vec{z}(x)\right) + \vec{\lambda}^T \left(\vec{\sigma}_t^0 - \mathcal{T}\left(\vec{U}(x)\right)\right)$$

is used. The gradient with respect to the wind field and $\vec{\lambda}$ are set to zero to find the critical points. Depending on the metric and the sampling geometry, a second derivative test may be required to distinguish the maxima from the minima. For a given set of noise-free measurements $\vec{\sigma}_t^0$, the solutions to these equations and inequality constraints represent the wind fields that are consistent with the forward operator that optimize the metric. As a function of $\vec{\sigma}_t^0$, the set of equations and inequalities defines

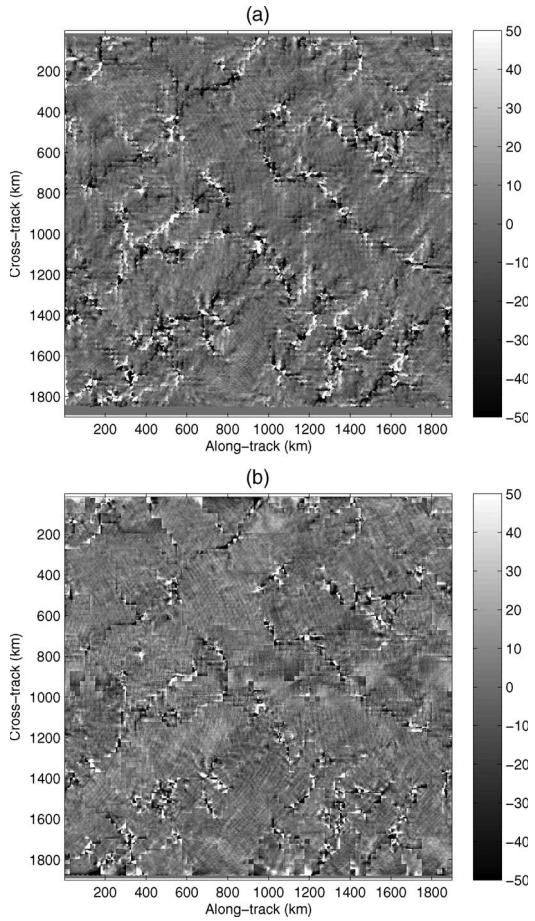

Fig. 9. Bias of the wind direction estimates (in degrees) for (a) MAP and (b) UHR.

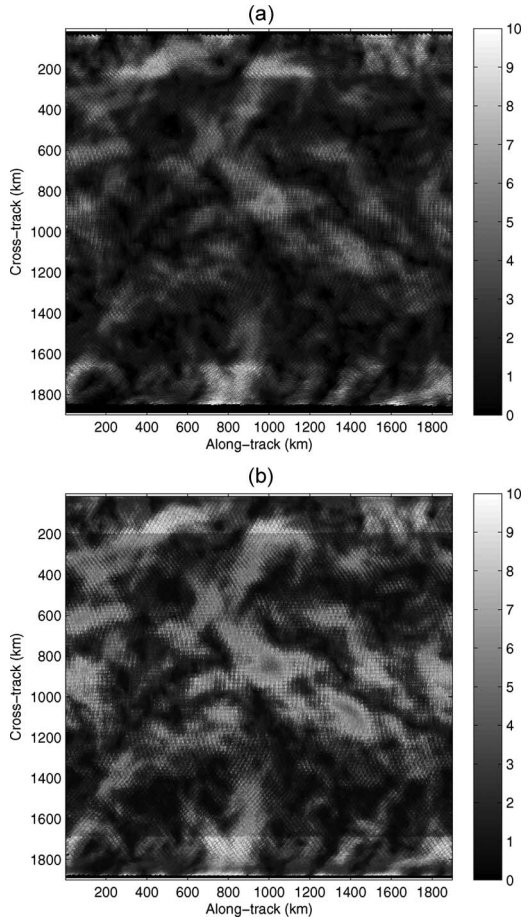

Fig. 10. STD of the wind speed estimates (in meters per second) for (a) MAP and (b) UHR.

a finite-dimensional manifold in the wind domain representing all consistent solutions that optimize the metric. This manifold defines the class of signals that can be reconstructed under the metric. A different metric may result in a different class of reconstructible signals. In principle, the manifold may be parameterized, producing a wind field model with finitely many parameters that can be estimated from the σ^0 measurements.

Note that, although this approach allows the reconstructible wind field signals to be represented with a finite number of parameters because of the nonlinearity, the manifold cannot, in general, be contained within the span of a finite linear basis. Since the bandlimited spaces are finite linear subspaces, the class of reconstructible wind fields is generally not bandlimited. Even if all of the aperture functions are bandlimited, they may not impose a bandlimit on the wind fields (nor on the σ^0 fields because they must be consistent with the wind field). Therefore, it may be possible to obtain wind estimates (and corresponding σ^0 field estimates) with a higher frequency content than the bandlimit of the aperture functions.

APPENDIX B
RELATIONSHIP BETWEEN SPECTRA OF THE WIND AND σ^0 FIELDS

This section presents the relationship between the wavenumber spectrum (Fourier transform) of the spatially continuous σ^0 fields for each measurement and the wavenumber spectrum of the components of the wind field. First, a theorem and a proof for the relationship between the spectrum of the σ^0 fields and the spectrum of the components of the wind field are stated. Then, some practical considerations for the relationship of the bandlimit of the σ^0 fields and the bandlimit of the wind fields are presented.

Theorem: For the nonlinear operator $\mathcal{T}$ defined in (1) with a GMF that can be represented by a finite power series (where N_1 and N_2 are the order of the wind vector components), we have the following.

1) The Fourier transform of the ith σ^0 field $\sigma_i(x) = \text{gmf}(\vec{U}(x), \theta_i(x), \psi_i(x))$ is related to the Fourier transform of the components of wind field $U_1(x)$ and $U_2(x)$ by

$$\mathcal{F}\{\sigma_i(x)\} = \sum_{n_1,n_2=0}^{N_1,N_2} \mathcal{F}\{a_{i,n_1,n_2}(x)\} * \left[\mathop{*}_{k=1}^{2} \left[\mathop{*}_{j=1}^{n_k} \mathcal{F}\{U_k(x)\} - \mathcal{F}\{c_k\} \right] \right] \quad (8)$$

where $\mathcal{F}$ represents the Fourier transform, $a_{i,n_1,n_2}(x)$ is the power series coefficient corresponding to $U_1(x)$ and $U_2(x)$, c_k represents a reference wind field component that is constant in x, and $*_{j=1}^{n}$ represents n nested convolutions.

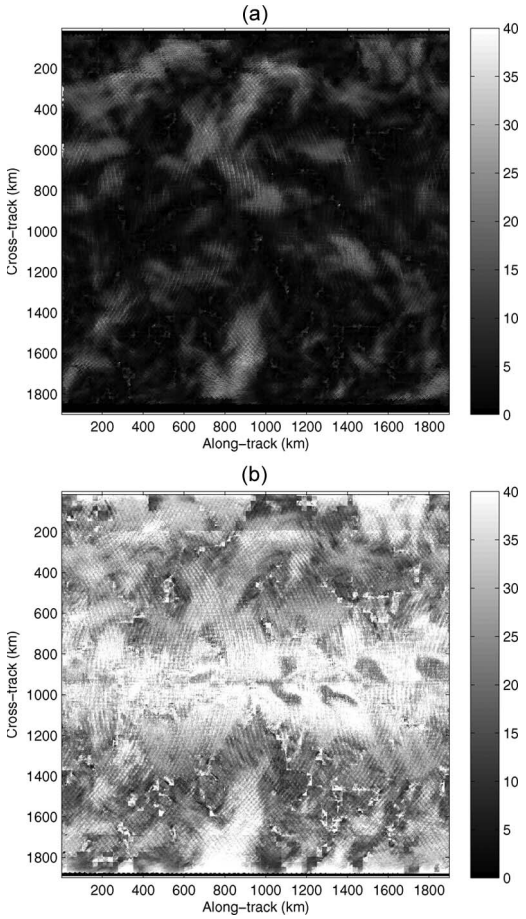

Fig. 11. STD of the wind direction estimates (in degrees) for (a) MAP and (b) UHR.

2) If the wind field components are bandlimited by ω_{U_1} and ω_{U_2} and the power series coefficients are bandlimited by ω_a, then the σ^0 field components are bandlimited by

$$\omega_\sigma \leq N_1\omega_{U_1} + N_2\omega_{U_2} + \omega_a. \tag{9}$$

Proof: Showing part 1) is straightforward. The power series expansion of $\sigma_i = \text{gmf}(\vec{U}(x), \theta_i(x), \psi_i(x))$ is

$$\sigma_i(x) = \sum_{n_1,n_2=0}^{N_1,N_2} a_{i,n_1,n_2}(x) \prod_{k=1}^{2} (U_k(x) - c_k)^{n_k}.$$

Taking the Fourier transform produces

$$\begin{aligned}\mathcal{F}\{\sigma_i(x)\} &= \mathcal{F}\left\{\sum_{n_1,n_2=0}^{N_1,N_2} a_{i,n_1,n_2}(x) \prod_{k=1}^{2} (U_k(x) - c_k)^{n_k}\right\} \\ &= \sum_{n_1,n_2=0}^{N_1,N_2} \mathcal{F}\{a_{i,n_1,n_2}(x)\} \\ &\quad * \mathcal{F}\left\{\prod_{k=1}^{2}\prod_{j=1}^{n_k} (U_k(x) - c_k)\right\} \\ &= \sum_{n_1,n_2=0}^{N_1,N_2} \mathcal{F}\{a_{i,n_1,n_2}(x)\} \\ &\quad * \left[\mathop{*}_{k=1}^{2}\left[\mathop{*}_{j=1}^{n_k} (\mathcal{F}\{U_k(x)\} - \mathcal{F}\{c_k\})\right]\right]\end{aligned}$$

which is (8).

To show part 2), we start with the bandlimited wind field components with bandlimits ω_{U_k} for each component k. Note that, since c_k is a constant for each k, $\mathcal{F}\{c_k\}$ is a delta function centered at zero. The term

$$\left[\mathop{*}_{j=1}^{n_k} (\mathcal{F}\{U_k(x)\} - \mathcal{F}\{c_k\})\right]$$

represents the convolution of the kth wind field component with itself n_k times, with the dc term modified. Each autoconvolution expands the spectrum by ω_{U_k}, so the term above has a bandlimit of $n_1\omega_{U_1}$ for $k = 1$. This term is then convolved with the autoconvolution of the other wind field component (i.e., $k = 2$), which has a bandlimit of $n_2\omega_{U_2}$, producing a bandlimit of $n_1\omega_{U_1} + n_2\omega_{U_2}$. This quantity is then convolved with $\mathcal{F}\{a_{i,n_1,n_2}(x)\}$, resulting in a bandlimit of $n_1\omega_{U_1} + n_2\omega_{U_2} + \omega_a$. Then, each combination of n_1 and n_2 is added together. The resulting bandlimit is the highest bandlimit of any of the terms in the sum, which corresponds to the term where $n_1 = N_1$ and $n_2 = N_2$, resulting in the bandlimit $N_1\omega_{U_1} + N_2\omega_{U_2} + \omega_a$. In case some high-frequency contents of the different terms in the sum cancel out portions of the spectrum, an inequality relation is obtained. Thus

$$\omega_\sigma \leq N_1\omega_{U_1} + N_2\omega_{U_2} + \omega_a.$$

■

Note that $a_{i,n_1,n_2}(x)$ is a function of x because the look geometry changes in x. If the aperture functions are sufficiently narrow such that a variation of the look geometry is negligible over the main lobe, then $a_{i,n_1,n_2}(x)$ can be approximated as constant in x, and the result in part 2) of the theorem reduces to

$$\omega_\sigma \leq N_1\omega_{U_2} + N_2\omega_{U_2}.$$

The relationship between the bandlimit of the σ^0 fields and the bandlimit of the wind field components suggests that an upsampled version of the wind field should be projected through the sampling operator when calculating the forward projection. Although the actual bandlimit of the σ^0 fields can be as high as the result in part 2) of the theorem, it may be possible to assume that the σ^0 bandlimit is similar to the bandlimit of the wind components without introducing significant errors. This is because the autoconvolutions in (8) tend to produce spectra with relatively low energy at high frequencies. To illustrate this, consider the 1-D case. The magnitude of the autoconvolution

of a bandlimited signal is less than the autoconvolution of the magnitude, i.e.,

$$\begin{aligned}|X(\omega) * X(\omega)| &= \left| \int X(\tau)X(\tau-\omega)d\tau \right| \\ &\leq \int |X(\tau)|\,|X(\tau-\omega)|\,d\tau \\ &= |X(\omega)| * |X(\omega)|\,.\end{aligned}$$

Also, note that $|X(\omega)| \leq \alpha B(\omega)$ for some α and for every ω, where $B(\omega)$ is a boxcar function centered at zero. Thus

$$\begin{aligned}|X(\omega) * X(\omega)| &\leq (\alpha B(\omega)) * |X(\omega)| \\ &\leq (\alpha B(\omega)) * (\alpha B(\omega)) = \alpha^2 (B(\omega) * B(\omega))\,.\end{aligned}$$

Extending this to multiple nested convolutions, we have

$$\left| \underset{j=1}{\overset{n}{*}} X(\omega) \right| \leq \alpha^n \underset{j=1}{\overset{n}{*}} B(\omega).$$

Now, consider the autoconvolution of the boxcar function. Each increasing n extends the tail into the higher frequencies, but the higher frequencies have lower values than the lower frequencies.

Appendix C
Gradient of the MAP Objective Function

The gradient of the MAP objective function is required for the practical implementation of the MAP wind reconstruction method. Here, the gradient of the MAP objective function is derived.

The MAP objective function is the sum of the log-likelihood function $\log f(\vec{\sigma_m^0}|\vec{\sigma_t^0})$ (or equivalently $\log f(\vec{\sigma_m^0}|\vec{U}[x])$) and the log of the prior $\log f(\vec{U}[x])$. For the scatterometer noise model used in this paper, the partial of the log-likelihood function with respect to the ith wind vector component at location x is

$$\begin{aligned}&\frac{\partial \log f\left(\vec{\sigma}_m^0|\vec{U}[x']\right)}{\partial U_i[x]} \\ &\quad = -\sum_n \frac{\partial}{\partial U_i[x]} \left[\frac{\left(\sigma_{m,n}^0 - T_n\left(\mathbf{H}\vec{U}[x']\right)\right)^2}{2R_{n,n}} \right. \\ &\qquad \left. + \frac{1}{2}\left(\log\{2\pi\} + \log\{R_{n,n}\}\right) \right]. \quad (10)\end{aligned}$$

The first term in the sum is

$$\begin{aligned}&\frac{\partial}{\partial U_i[x]} \left[\frac{\left(\sigma_{m,n}^0 - T_n\left(\mathbf{H}\vec{U}[x']\right)\right)^2}{2R_{n,n}} \right] \\ &\quad = -\frac{\left(\sigma_{m,n}^0 - T_n\left(\mathbf{H}\vec{U}[x']\right) A_n[x] \frac{\partial \mathrm{gmf}_n\left(\vec{U}[x]\right)}{\partial U_i[x]}\right)}{R_{n,n}} \\ &\qquad - \frac{\left(\sigma_{m,n}^0 - T_n\left(\mathbf{H}\vec{U}[x']\right)\right)^2}{2R_{n,n}^2} \frac{\partial R_{n,n}}{\partial U_i[x]}\end{aligned}$$

where $T_n = \sum_y A_n[y]\mathrm{gmf}_n(\mathbf{H}\vec{U}[x'])$. The second term in the sum in (10) is

$$\frac{\partial}{\partial U_i[x]} \frac{1}{2}\left[\log\{2\pi\} + \log\{R_{n,n}\}\right] = \frac{1}{2R_{n,n}} \frac{\partial R_{n,n}}{\partial U_i[x]}.$$

Note that the partial derivative of $R_{n,n}$ is

$$\frac{\partial R_{n,n}}{\partial U_i[x]} = \left(2\alpha_n T_n\left(\mathbf{H}\vec{U}[x']\right) + \beta_n\right) A_n[x] \frac{\partial \mathrm{gmf}_n\left(\vec{U}[x]\right)}{\partial U_i[x]}.$$

Thus

$$\frac{\partial \log f\left(\vec{\sigma}_m^0|\vec{U}[x']\right)}{\partial U_i[x]} = \sum_n -K_n A_n[x] \frac{\partial \mathrm{gmf}_n\left(\vec{U}[x]\right)}{\partial U_i[x]} \quad (11)$$

where

$$\begin{aligned}K_n = \Bigg[&\frac{\left(\sigma_{m,n}^0 - T_n\left(\mathbf{H}\vec{U}[x']\right) - \left(\alpha_n T_n\left(\mathbf{H}\vec{U}[x']\right) + \beta_n/2\right)\right.}{R_{n,n}} \\ &+ \frac{\left(\sigma_{m,n}^0 - T_n\left(\mathbf{H}\vec{U}[x']\right)^2 \left(\alpha_n T_n\left(\mathbf{H}\vec{U}[x']\right) + \beta_n/2\right)\right.}{R_{n,n}^2} \Bigg].\end{aligned}$$

The gradient of the log of the prior expressed in (5) and (6) is

$$\begin{aligned}&\frac{\partial \log f\left(\vec{U}[x']\right)}{\partial U_i[x]} \\ &\qquad = \sum_n \frac{-1}{p}\left(\sigma_n^0 - \mathrm{gmf}_n\left(\vec{U}[x]\right)\right) \frac{\partial \mathrm{gmf}_n\left(\vec{U}[x]\right)}{\partial U_i[x]}.\end{aligned}$$

Adding this expression to (11) results in the gradient of the MAP objective function.

References

[1] T. Lungu, *QuikSCAT Science Data Product Users Manual Overview and Geophysical Data Products*. Pasadena, CA: JPL, Sep. 2006.

[2] *ASCAT Wind Product User Manual*, KNMI, De Built, 2009.

[3] B. W. Stiles, S. M. Hristova-Veleva, R. S. Dunbar, S. Chan, S. L. Durden, D. Esteban-Fernandez, E. Rodriguez, W. L. Poulsen, R. W. Gaston, and P. S. Callahan, "Obtaining accurate ocean surface winds in hurricane conditions: A dual-frequency scatterometry approach," *IEEE Trans. Geosci. Remote Sens.*, vol. 48, no. 8, pp. 3101–3113, Aug. 2010.

[4] A. Stoffelen and M. Portabella, "On Bayesian scatterometer wind inversion," *IEEE Trans. Geosci. Remote Sens.*, vol. 44, no. 6, pp. 1523–1533, Jun. 2006.

[5] B. W. Stiles, B. D. Pollard, and R. S. Dunbar, "Direction interval retrieval with thresholded nudging: A method for improving the accuracy of QuikSCAT winds," *IEEE Trans. Geosci. Remote Sens.*, vol. 40, no. 1, pp. 79–89, Jan. 2002.

[6] A. Stoffelen and D. Anderson, "Ambiguity removal and assimilation of scatterometer data," *Q. J. R. Meteorol. Soc.*, vol. 123, no. 538, pp. 491–518, Jan. 1997.

[7] H. Roquet and A. Ratier, "Towards direct variational assimilation of scatterometer backscatter measurements into numerical weather prediction models," in *Proc. Int. Geosci. Remote Sens. Symp.*, Edinburgh, U.K., 1988, pp. 257–260.

[8] A. Stoffelen, S. de Haan, Y. Quilfen, and H. Schyburg, "ERS scatterometer ambiguity removal scheme comparison," OSISAF, EUMETSAT, Darmstadt, Germany, Tech. Rep., 2000.
[9] D. Cornford, G. Ramage, and I. T. Nabney, "A scatterometer neural network sensor model with input noise," *Neurocomputing*, vol. 30, no. 1–4, pp. 13–21, Jan. 2000.
[10] R. N. Hoffmann, S. M. Leidner, J. M. Hendersom, R. Atlas, J. V. Ardizzone, and S. C. Bloom, "A two-dimensional variational analysis method for NSCAT ambiguity removal: Methodology, sensitivity, and tuning," *J. Atmos. Ocean. Technol.*, vol. 20, no. 5, pp. 585–605, May 2003.
[11] M. Portabella and A. Stoffelen, "A probabilistic approach for SeaWinds data assimilation," *Q. J. R. Meteorol. Soc.*, vol. 130, no. 596, pp. 127–152, Jan. 2004.
[12] J. Vogelzang, A. S. A. Verhoef, J. de Vries, and H. Bonekamp, "Validation of two-dimensional variational ambiguity removal on SeaWinds scatterometer data," *J. Atmos. Ocean. Technol.*, vol. 26, no. 7, pp. 1229–1245, Jul. 2009.
[13] M. Portabella and A. Stoffelen, "Scatterometer backscatter uncertainty due to wind variability," *IEEE Trans. Geosci. Remote Sens.*, vol. 44, no. 11, pp. 3356–3362, Nov. 2006.
[14] B. A. Williams, M. P. Owen, and D. G. Long, "The ultra high resolution QuikSCAT product," in *Proc. IEEE Radar Conf.*, Pasadena, CA, May 2009, pp. 1–6.
[15] A. M. Plagge, D. C. Vandemark, and D. G. Long, "Coastal validation of ultra-high resolution wind vector retrieval from QuikSCAT in the Gulf of Maine," *IEEE Geosci. Remote Sens. Lett.*, vol. 6, no. 3, pp. 413–417, Jul. 2009.
[16] D. G. Long, "Wind field model-based estimation of SEASAT scatterometer winds," *J. Geophys. Res.*, vol. 98, no. C8, pp. 14 651–14 688, Aug. 1993.
[17] D. G. Long and J. M. Mendel, "Model-based estimation of wind fields over the ocean from scatterometer measurements part I: The wind field model," *IEEE Trans. Geosci. Remote Sens.*, vol. 28, no. 2, pp. 349–360, May 1990.
[18] D. G. Long and J. M. Mendel, "Model-based estimation of wind fields over the ocean from scatterometer measurements part II: Estimation of the model parameters," *IEEE Trans. Geosci. Remote Sens.*, vol. 28, no. 2, pp. 361–373, May 1990.
[19] D. G. Long, P. J. Hardin, and P. T. Whiting, "Resolution enhancement of spaceborne scatterometer data," *IEEE Trans. Geosci. Remote Sens.*, vol. 31, no. 3, pp. 700–715, May 1993.
[20] D. S. Early and D. G. Long, "Image reconstruction and enhanced resolution imaging from irregular samples," *IEEE Trans. Geosci. Remote Sens.*, vol. 39, no. 2, pp. 291–302, Feb. 2001.
[21] B. A. Williams and D. G. Long, "Scatterometer image reconstruction from aperture-filtered samples," in *Proc. Int. Geosci. Remote Sens. Symp.*, Honolulu, HI, Jul. 2010, pp. 1835–1838.
[22] B. A. Williams and D. G. Long, "Reconstruction from aperture-filtered samples with application to scatterometer image reconstruction," *IEEE Trans. Geosci. Remote Sens.*, vol. 49, no. 5, pp. 1663–1676, May 2011.
[23] A. V. Oppenheim and R. W. Schafer, *Discrete-Time Signal Processing*, A. V. Oppenheim, Ed., 2nd ed. Upper Saddle River, NJ: Prentice-Hall, 1999.
[24] H. G. Feichtinger and K. Grochenig, "Irregular sampling theorems and series expansions of band-limited functions," *J. Math. Anal. Appl.*, vol. 167, no. 2, pp. 530–556, Jul. 1992.
[25] F. T. Ulaby, R. K. Moore, and A. K. Fung, *Microwave Remote Sensing*, vol. 1. Norwood, MA: Artech House, 1981.
[26] M. W. Spencer and D. G. Long, "High resolution measurements with a spaceborne pencil-beam scatterometer using combined range/Doppler discrimination techniques," *IEEE Trans. Geosci. Remote Sens.*, vol. 41, no. 3, pp. 567–581, Mar. 2003.
[27] F. T. Ulaby, R. K. Moore, and A. K. Fung, *Microwave Remote Sensing*, vol. 2. Norwood, MA: Artech House, 1981.
[28] M. H. Freilich and D. B. Chelton, "Wavenumber spectra of pacific winds measured by the SEASAT scatterometer," *J. Phys. Oceanogr.*, vol. 16, no. 4, pp. 741–757, Apr. 1986.
[29] R. E. Fischer, "Standard deviation of scatterometer measurements from space," *IEEE Trans. Geosci. Electron.*, vol. GE-10, no. 2, pp. 106–113, Apr. 1972.
[30] M. W. Spencer and D. G. Long, "Radar backscatter measurement accuracy for a spaceborne pencil-beam wind scatterometer with transmit modulation," *IEEE Trans. Geosci. Remote Sens.*, vol. 35, no. 1, pp. 102–114, Jan. 1997.
[31] D. G. Long and J. M. Mendel, "Identifiability in wind estimation from wind scatterometer measurements," *IEEE Trans. Geosci. Remote Sens.*, vol. 29, no. 2, pp. 268–276, Mar. 1991.
[32] T. D. Moon and W. C. Stirling, *Mathemetical Methods and Algorithms for Signal Processing*, T. Robbins, Ed. Upper Saddle River, NJ: Prentice-Hall, 2000.
[33] B. A. Williams and D. G. Long, "Hurricane wind field estimation from SeaWinds at ultra high resolution," in *Proc. IGARSS*, 2007, pp. 1075–1078.
[34] M. Portabella and A. Stoffelen, "Scatterometer backscatter uncertainty due to wind variability," *IEEE Trans. Geosci. Remote Sens.*, vol. 44, no. 11, pp. 3356–3362, Nov. 2006.
[35] T. M. Cover and J. A. Thomas, *Elements of Information Theory,* 2nd ed. Hoboken, NJ: Wiley Interscience, 2005.
[36] B. A. Williams, "Signal processing methods for ultra high resolution scatterometry," Ph.D. dissertation, Brigham Young Univ., Provo, UT, 2010.
[37] C.-Y. Chi and F. K. Li, "A comparative study of several wind estimation algorithms for spaceborne scatterometers," *IEEE Trans. Geosci. Remote Sens.*, vol. 26, no. 2, pp. 115–121, Mar. 1988.
[38] I. S. Ashcraft and D. G. Long, "The spatial response function of SeaWinds backscatter measurements," in *Proc. SPIE*, W. L. Barnes, Ed., Aug. 2003, vol. 5151, pp. 609–618.

Brent A. Williams (M'04) received the B.S. and Ph.D. degrees in electrical engineering from the Brigham Young University, Provo, UT, in 2005 and 2010, respectively. He has recently finished his dissertation entitled "Signal Processing Methods for Ultra High Resolution Scatterometry."

From 2005 to 2010, he worked in the Microwave Earth Remote Sensing Laboratory, exploring ultrahigh-resolution ocean wind scatterometry and σ^0 image reconstruction. He is currently with the Jet Propulsion Laboratory, Pasadena, CA, continuing research in scatterometry.

Dr. Williams is a member of the Eta Kappa Nu. He received the IEEE Geoscience and Remote Sensing Society Interactive Session Prize Paper Award in 2006 and the IEEE Geoscience and Remote Sensing Society Mikio Takagi Student Prize Award in 2007 and 2010.

David G. Long (S'80–SM'98–F'08) received the Ph.D. degree in electrical engineering from the University of Southern California, Los Angeles, in 1989.

From 1983 to 1990, he was with NASA's Jet Propulsion Laboratory (JPL), where he developed advanced radar remote sensing systems. While at JPL, he was the Project Engineer on the NASA Scatterometer (NSCAT) project which flew from 1996 to 1997. He also managed the SCANSCAT project, which is the precursor to SeaWinds, which was launched in 1999 and 2002. He is currently a Professor with the Electrical and Computer Engineering Department, Brigham Young University, Provo, UT, where he teaches upper division and graduate courses in communications, microwave remote sensing, radar, and signal processing and where he is the director of the BYU Center for Remote Sensing. He is the Principal Investigator on several NASA-sponsored research projects in remote sensing. He has over 390 publications in signal processing and radar scatterometry. His research interests include microwave remote sensing, radar theory, space-based sensing, estimation theory, signal processing, and mesoscale atmospheric dynamics.

Dr. Long is currently an Associate Editor of the IEEE GEOSCIENCE AND REMOTE SENSING LETTERS. He has received the NASA Certificate of Recognition several times.